Influence of disorder on the optical absorption in semiconductors: Application to epitaxially grown III-V compounds

K. Dziatkowski,* Ł. Cywiński, W. Bardyszewski, and A. Twardowski
Faculty of Physics, Warsaw University, Hoża 69, 00-681 Warsaw, Poland

H. Saito and K. Ando
Nanoelectronics Research Institute, National Institute of Advanced Industrial Science and Technology, Tsukuba Central 2 Umezono 1-1-1, Tsukuba, Ibaraki 305-8568, Japan

(Received 13 January 2006; revised manuscript received 8 May 2006; published 21 June 2006)

The influence of disorder on optical properties of semiconductors is discussed in different models: phenomenological model of partially relaxed **k**-selection rule, spectral density model, and the model taking into account excitonic effects. These models were compared to experimental spectra of disordered GaAs, where disorder was generated either by MBE low temperature growth or by implantation of arsenic. Reasonable agreement between the data and the models was obtained. The analysis of the data supports the view that the main source of disorder in nonstoichiometric GaAs are the defects resulting from the excessive arsenic, e.g., arsenic antisites.

DOI: 10.1103/PhysRevB.73.235340 PACS number(s): 78.66.Fd, 75.50.Pp

I. INTRODUCTION

Despite many successful applications, the generally known and appreciated model of semiconductors based on the assumption of infinite defectless crystal is an obvious simplification, since dynamic and static disorder is permanently present in real systems. There are many physical phenomena, such as the quantum Hall effect, whose manifestation is closely related to disorder and whose theoretical description requires the breaking of ideal translational symmetry to be included. Therefore understanding the influence of disorder on the properties of semiconductors is one of the most key issues of solid state physics.

Magnetic III-V compounds, which belong to a wide class of diluted magnetic semiconductors (DMSs), can serve as an example of disordered systems. In such mixed crystals a part of nonmagnetic cations of the host material (GaAs, InSb, etc.) is replaced by manganese atoms, thus the understanding of crystalline disorder is of particular importance for physical properties of III-Mn-V compounds.[1] Recently many theoretical studies claimed the influence of disorder on magnetic,[2–4] transport,[4] or optical properties[5] of GaMnAs, which is currently the most interesting representative of III-Mn-V alloys.

In the case of GaMnAs incorporation of a significant amount (over 1 mol %) of the magnetic ions into the GaAs host is impossible using classical bulk or molecular beam epitaxy (MBE) growth. This limitation was circumvented by so-called low temperature (LT) epitaxy, i.e., GaMnAs is usually obtained at 200–300 °C, while the high purity GaAs is grown by MBE method at 500–600 °C.[6] However, LT-MBE growth of GaMnAs is a source of additional defects, interstitial manganese (Mn_I),[7] and arsenic substituting gallium (As_{Ga}),[8] thus increasing structural disorder of this material.

The most convenient method of investigating the effect of disorder on the band structure employs optical absorption studies. Typically the absorption coefficient measured for below-the-energy-gap photon energies reveals exponential fall-off, the Urbach edge, while for high energies the square-root dependence (as in a bulk, perfect crystal) is observed. In the crossover region one may expect a parabolic behavior

$$\alpha(E) \sim \frac{(E-E_g)^2}{E}, \tag{1}$$

called the Tauc edge. The physical mechanism which stands behind the Tauc edge is still unexplained. It is believed that in this energy range the absorption takes place between the delocalized states disturbed by disorder.[9] Lasher and Stern[10] proposed the model of absorption spectra in disordered semiconductor above the Urbach region, assuming that the absorption coefficient $\alpha(E)$ is proportional to the convolution of the densities of states in conduction and valence bands ρ_c and ρ_v multiplied by the effective matrix element $\mathcal{M}$ and the occupation number factor $f(E')-f(E'+E)$:

$$\alpha(E) \sim \int_{-\infty}^{+\infty} dE' \rho_v(E')\rho_c(E'+E) \times \mathcal{M}^2(E',E'+E)[f(E')-f(E'+E)]. \tag{2}$$

It has to be stressed that the model is purely phenomenological and no derivation of this popular formula exists. Similar approaches, with different densities of states and different empirical matrix elements, were used throughout many years.[11–13]

Several results of optical experiments concerning the vicinity of the fundamental absorption edge were reported for amorphous and crystalline, disordered semiconductors.[14–16] Also mixed, semimagnetic compounds were investigated, and in the case of $Ga_{1-x}Mn_xAs$ epilayers the absorption spectrum appeared nearly linear in energy.[17] A similar ramplike edge was also found for pure GaAs grown at low temperatures (LT-GaAs),[18] which leads to the question of whether the presence of manganese contributes in making the linear energy spectrum of GaMnAs which is already disordered by As_{Ga} antisites. Thorough optical studies of GaAs with antistructural As_{Ga} defects may be helpful in solving this prob-

TABLE I. Investigated samples.

Low-temperature GaAs					
Name	LT1	LT2	LT3	LT4	LT5
Growth temperature (°C)	250	275	300	400	500
GaAs implanted with arsenic					
Name	IM1	IM2	IM3	IM4	IM5
Annealing temperature (°C)	[a]	500	520	600	700

[a]As implanted.

lem. In general there are two ways to obtain arsenic reach GaAs: low temperature growth or arsenic implantation.[19,20] The optical properties of both materials in the below-the-gap region have been studied intensively due to optoelectronic applications,[21] however, understanding of the above-the-gap range of the spectrum is still limited.[22]

In this paper we present the optical measurements of the fundamental absorption edge of disordered GaAs layers. The results are discussed on the basis of two developed models of interband absorption in disordered semiconductors. The first one is the improved empirical method proposed in Ref. 17 using the partially relaxed **k**-selection rule (RkR) for single particle transitions, while the other one is based on the cumulant expansion approximation of the excitonic absorption edge. Both models are successfully applied to collected experimental data of the absorption.

II. EXPERIMENTAL

In order to isolate the main source of disorder in $Ga_{1-x}Mn_xAs$ we use two types of disordered GaAs samples without manganese (see Table I). The first ones were 0.7-μm-thick low temperature GaAs layers (LT-GaAs) grown on a sapphire substrate in a molecular beam epitaxy system. The temperature of the substrate was varied in the range of 250–500 °C. The second group were 2.5-μm-thick GaAs epilayers implanted with arsenic. At 700 °C they were deposited with a metalorganic chemical vapor deposition method on AlAs buffer following "epiready" SI-GaAs substrate. These samples were annealed at different temperatures in the range of 500–700 °C, then mounted on glass supports, and finally the substrates were removed in order to enable the optical experiments in the region of the fundamental absorption edge of GaAs. The additional data about investigated implanted films may be found in Ref. 23.

Typical optical absorption measurements were performed with a commercial UV-FIR spectrophotometer. The investigated spectral range obtained with the use of a tungsten lamp covered the photon energy from 1 to 2 eV. The samples were mounted in the cryostat equipped with a "cold finger" holder and a helium microrefrigerator providing the temperature range from 12 to 300 K. For each layer two absorbance spectra were recorded at ambient and 12 K temperature.

III. RESULTS

A. Low-temperature GaAs

In the upper-row panels of Fig. 1 the absorbance spectra of LT-GaAs samples measured at 12 K are presented. For the entire range of the growth temperature T_g there is no significant change of the shape of spectra, which (neglecting the interference fringes) are almost structureless with no appearance of the fundamental absorption edge. For higher T_g (samples LT4 and LT5) a small kink at 1.8 eV is visible. Its position and disappearance in experiments made at 300 K suggest that the kink might be regarded as a weak manifestation of the split-off subband, but strongly pronounced interference fringes, that are present well above the energy gap of pure GaAs in all LT spectra, make the interpretation of these remanent structures very tentative.[24] One may suspect two sources of disorder to cause the ramplike shape of the absorption edge of LT-GaAs samples: an excess of arsenic and the strain between GaAs layer and the substrate. The

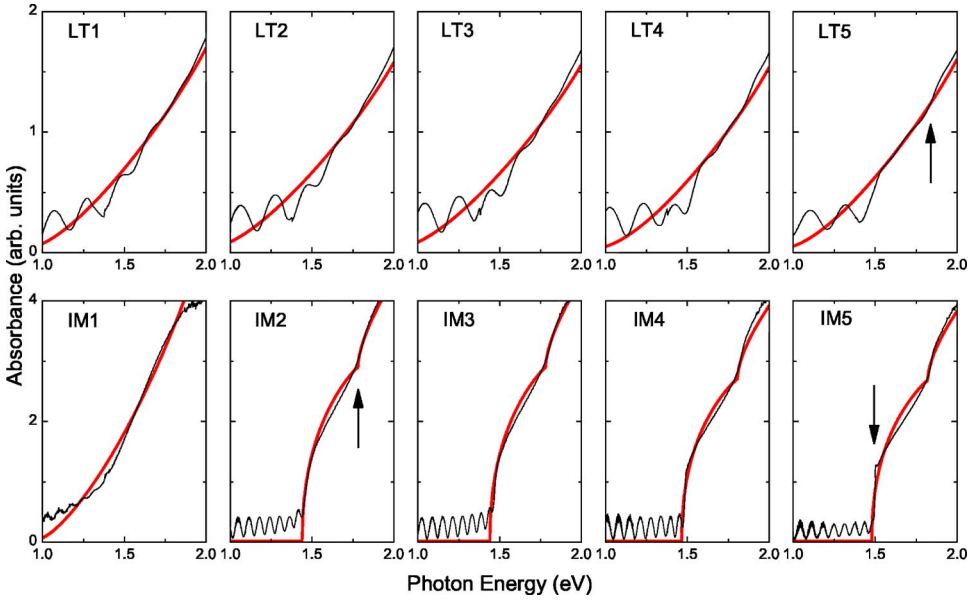

FIG. 1. (Color online) Upper row: Experimental absorbance spectra measured at 12 K (black) and theoretical curves fitted with RkR model (red) of low temperature GaAs. An arrow at about 1.8 eV of LT5 panel marks a possible manifestation of the split-off subband. Lower row: same as above for arsenic implanted GaAs. At about 1.5 eV of IM5 panel an emerged excitonic peak is indicated by the arrow.

latter is probably more important in the case of GaAs grown on sapphire as compared to the samples grown on lattice-matched SI-GaAs. While the concentration of antisite As_{Ga} defects are expected to diminish with rising growth temperature T_g, the strain is rather weakly affected by T_g and remains even for high-temperature grown films.

B. GaAs implanted with arsenic

The lower-row panels of Fig. 1 show the spectra of implanted GaAs collected at 12 K. In contrast to the results obtained for LT-GaAs, the evolution of the fundamental absorption edge induced by annealing is clearly visible: the higher annealing temperature T_{ann}, the spectra become sharper and for $T_{ann}=700\,^{\circ}C$ the excitonic peak appears around 1.5 eV. Simultaneously the split-off subband becomes more pronounced around 1.8 eV and the magnitude of absorbance in the entire investigated spectral range goes down.[25]

The below-the-gap region of the spectra, although dominated by the interference fringes, shows some additional component of the absorption, which magnitude increases with lowering T_{ann}, and finally for as implanted (IM1) sample forms a distinct tail extending far outside the spectral range investigated in our paper. This additional contribution may have both interband or defect origin. As we mentioned in the introduction, for below-the-gap range one expects to find so-called Urbach edge, i.e., an exponential dependence of the absorption on the photon energy, which is resembled by the tails observed in our study. On the other hand, in GaAs there is the well known EL2 (As_{Ga} antisite) defect, that contributes to the absorption of GaAs below its fundamental edge.[26] While at low temperatures the absorption from As_{Ga} is usually expected to be quenched by illumination with 1.0–1.3 eV light, in the case of our implanted samples no effect of illumination on the absorption was observed. However, one should not regard this quenching as a general hallmark of arsenic reach GaAs, since in plastically deformed GaAs a similar below-the-gap absorption band undergoes no illumination-induced reduction, even though the intensity of the band rises with the increasing concentration of As_{Ga} defects.[27] The absorbance spectra measured at 300 K show analogous dependence on T_{ann} as above described data for 12 K, with less visible split-off subband for all epilayers and with no excitonic peak for the IM5 sample.[24]

IV. DISCUSSION

In the following section we provide a more insightful discussion of the observed spectra and their dependence on the growth or annealing temperature. For that purpose two quantitative models of the interband absorption are applied to the collected experimental data.

A. Model of partially relaxed *k*-selection rule (RkR)

Szczytko *et al.*[17] proposed an empirical model of absorption in random media based on disorder induced by the partial relaxation of the **k**-selection rule.[29] Here we improve their idea of indirect interband transitions with the isotropic (in the **k** space), Gaussian distribution of the change of quasimomentum vector

$$\left(\frac{2\pi}{\sigma_k'^2}\right)^{3/2}\exp\left[-\frac{(\mathbf{k}_c-\mathbf{k}_v)^2}{2\sigma_k^2}\right], \tag{3}$$

by introducing the σ_k' parameter describing the change of the total magnitude of the matrix element $\mathcal{M}(\mathbf{k}_c,\mathbf{k}_v)$ in Eq. (2). There is no real argument why $\mathcal{M}(\mathbf{k}_c,\mathbf{k}_v)=\mathcal{M}(\Delta\mathbf{k})$ should be normalized to unity in $\Delta\mathbf{k}$ space (as proposed in Ref. 17), that is why σ_k' should equal σ_k in the general case, especially for large disorder. For instance, in the limit $\sigma_k'=\sigma_k\to\infty$ the distribution given by Eq. (3) vanishes, while the constant, nonzero value is expected,[10,17] which one obtains keeping finite value of σ_k' when σ_k approaches infinity.[30] In the opposite case of diminishing disorder one can expect $\sigma_k'\simeq\sigma_k$, thus for perfectly ordered crystal ($\sigma_k\to 0$) Dirac's δ distribution is recovered by Eq. (3). It will be shown later that the correct behavior of $\mathcal{M}(\Delta\mathbf{k})$ in the limits of small and large disorder is of particular importance for description of the absorption data presented in this paper.

Assuming parabolic bands and sufficiently low temperature that $f(E')-f(E'+E)\approx 1$ [Eq. (2)], the absorption coefficient in this model is given by[17]

$$\alpha(E)=A^2\frac{2m_v\sigma_k^2}{(2\pi)^{5/2}\hbar^2\sigma_k'^3}\int_0^{k_c^{\max}}dk_c k_c \times\left[\exp\left(-\frac{(k_c-k_v)^2}{2\sigma_k^2}\right)-\exp\left(-\frac{(k_c+k_v)^2}{2\sigma_k^2}\right)\right],$$

$$A^2=\frac{2\pi e^2\hbar E_p}{6cm_0\epsilon_0 nE},$$

$$k_v=\sqrt{\frac{2m_v}{\hbar^2}\left(E-E_g-\frac{\hbar^2k_c^2}{2m_c}\right)},\quad k_c^{\max}=\sqrt{\frac{2m_c}{\hbar^2}(E-E_g-F)}, \tag{4}$$

where m_c, k_c and m_v, k_v denote the effective mass and the quasimomentum vector of electron in conduction (c) and valence (v) bands, E_g is the band gap energy, F is the Fermi level energy measured from the top of the valence band, n is the refractive index, and E_p is the Kane energy parameter which for SI-GaAs equals 26 eV.[28] The above formula is valid only for a two-band semiconductor, while the energy structure of GaAs is more complicated. To obtain the absorption involving the entire valence band one should add the contributions from all three valence subbands of GaAs with adequate weights ($1:\frac{1}{3}:\frac{2}{3}$ for heavy, light and split-off holes reflecting the transition probabilities at Γ point of the Brillouin zone) taking into account the different effective masses of carriers and $E_g+\Delta_{SO}$ as the band gap energy value for split-off subband.[31]

Although Eq. (4) combines the absorption coefficient $\alpha(E)$ and the refractive index $n(E)$, the original model of Ref. 17 does not take into account the mutual coupling of these two quantities via the Kramers-Kronig (KK) relation

$$n(E) = 1 + \frac{\hbar c}{\pi} \int_0^\infty dE' \frac{\alpha(E')}{E'^2 - E^2}. \quad (5)$$

Here we satisfy this coupling by self-consistent calculations of the absorption coefficient, in each case applying 15 repetitions of the loop consisting of Eqs. (4) and (5). With this number of repetitions we provide necessary stability of the resulting absorption spectrum $\alpha(E)$, which is then transformed to the absorbance $\mathcal{A}(E)$ according to the formula

$$\mathcal{A}(E) = -\log_{10} \frac{(1-r_1^2)(1-r_2^2)e^{-\alpha d}}{(1-r_1 r_2 e^{-\alpha d})^2 + 4 r_1 r_2 e^{-\alpha d} \sin^2\left(\frac{Edn}{\hbar c}\right)},$$

$$r_1(E) = \frac{n(E)/n_s - 1}{n(E)/n_s + 1}, \quad r_2(E) = \frac{n(E) - 1}{n(E) + 1}, \quad (6)$$

where both the absorption in the volume of the sample as well as multiple reflections on the frontiers of plane-parallel film are included. Note different reflection coefficients r_1, r_2 for layer/substrate and layer/vacuum interfaces. For the former the following refraction indices of the substrate $n_s = 1.75$ and $n_s = 1.5$ were used in the case of LT-GaAs/sapphire and implanted-GaAs/glass interfaces respectively.[32] The integral in Eq. (5) cannot be fully evaluated since the measured absorbance spectrum is available only in the finite range of the photon energy ($E_{\min}$–$E_{\max}$). Therefore for $E < E_{\min}$ we put $\alpha \equiv 0$ and the numerical integral is limited to 0 and $E_{\max}$, while the contribution from $E_{\max}$–∞ range is added as the approximated value

$$N \int_{E_{\max}}^\infty dE' \frac{(E' - E_g)^{3/2}}{E'(E'^2 - E^2)} \approx N \int_{E_{\max}}^\infty dE' \frac{(E' - E_g)^{1/2}}{E'^2} \quad (7)$$

assuming for $E > E_{\max}$ the same absorption as for nondisordered system [the scaling factor N provides functional continuity of $\alpha(E)$ at $E_{\max}$]. Finally the fitting parameters are optimized with the least squares method in order to match the absorbance spectrum of Eq. (6) with an experimental one $\mathcal{A}_{\exp}$: the parameters are varied with the constant steps (0.005×10^9 m^{-1} for σ_k and σ_k', 0.005 eV for E_g) until the minimum of the following norm:

$$\sum_{E=1\ \mathrm{eV}}^{2\ \mathrm{eV}} [\mathcal{A}(E) - \mathcal{A}_{\exp}(E)]^2 \quad (8)$$

is reached.

The analysis of the absorbance spectra depicted in Fig. 1 suggests that all the results may be divided into two groups. The samples IM2–IM5 reveal sharp edge about 1.4–1.5 eV and clearly pronounced contribution from split-off subband about 1.8 eV, both typical for low level of disorder, whereas the spectra of the other six samples (IM1 and LT1–LT5) are almost structureless "ramps" resembling earlier results of the absorption measurements in highly disordered crystalline or amorphous semiconductors.[15] On that basis one can ascribe these two groups to the above mentioned limiting cases of disorder in the RkR model. The spectra of the samples IM2–IM5 correspond to $\sigma_k, \sigma_k' \to 0$, which in our case of numerical calculations must be approximated by the finite values of $\sigma_k = 0.05 \times 10^9$ m^{-1} and $\sigma_k' = 0.04 \times 10^9$ m^{-1}, respectively (Table II). While 0.05×10^9 m^{-1} is the smallest value of σ_k providing numerical stability of the RkR model, the value of $\sigma_k' = 0.04 \times 10^9$ m^{-1} was obtained from the fitting procedure applied to the spectra of IM2–IM5 samples. In all four cases the algorithm returned the same value of σ_k' (with varying parameter of the energy gap, E_g). On the other hand, the samples IM1 and LT1–LT5 may be well fitted in a limit of infinite disorder, i.e., $\sigma_k \to \infty$ or $\mathcal{M}(\mathbf{\Delta k}) = \text{const}$. We have already claimed that in this case σ_k' has a finite value and together with E_g may be used as a fitting parameter of the RkR model. In Table II the resulting values of E_g and σ_k' are collected for both groups of samples, and the corresponding fitted spectra are depicted with red color in Fig. 1.

TABLE II. The parameters of RkR model [Eq. (4)] applied to the spectra of investigated samples.

Low-temperature GaAs			
Name	σ_k (10^9 m^{-1})	σ_k' (10^9 m^{-1})	E_g (eV)
LT1	∞	1.525	0.880
LT2	∞	1.625	0.850
LT3	∞	1.635	0.850
LT4	∞	1.565	0.920
LT5	∞	1.535	0.915
GaAs implanted with As			
Name	σ_k (10^9 m^{-1})	σ_k' (10^9 m^{-1})	E_g (eV)
IM1	∞	1.580	0.930
IM2	0.05	0.040	1.440
IM3	0.05	0.040	1.440
IM4	0.05	0.040	1.465
IM5	0.05	0.040	1.480

In the case of low-temperature samples one finds theoretical spectra in an overall agreement with the experimental data, as shown in the upper row of Fig. 1. Neglecting the interference fringes the ramplike shape is correctly reproduced, and the already noted lack of influence of the growth temperature is confirmed by the parameters collected in Table II, which show no significant dependence on T_g. The disorder originating from the strain between LT-GaAs and unmatched sapphire substrate seems to override defect-induced relaxation of the interband selection rules, and since the former source of disorder is independent of T_g, one finds the ramplike absorption edge not really affected by the growth conditions.

For implanted and annealed GaAs (IM2–IM5) a reasonable matching between experimental data and theoretical results was obtained, with one essential deviation. The excitonic peak around 1.5 eV of the spectrum of IM5 sample is not reproduced, which is not surprising as the electron-hole Coulomb interaction was neglected in the RkR model. This problem will be addressed in Sec. IV B 4 by introducing the cumulant expansion approximation of the excitonic absorption edge.

The comprehensive analysis of the dependence of disorder on the annealing or growth temperature is impeded by the above mentioned fact that samples investigated in this study represent two extrema of the possible magnitude of disorder. Nevertheless some general quantitative behavior may be still rendered, e.g., for the energy gap that obviously correlates with the annealing temperature. Starting from the IM5 sample which absorption spectrum exhibits least disorder the energy gap is reduced as the annealing temperature decreases (i.e., the level of disorder is increased). Unsurprisingly, the renormalized energy gap reaches its minimum for as implanted GaAs (IM1), and as seen from the last column of Table II, the variation of E_g parameter itself may be used as a measure of disorder. Note that the value of $E_g = 0.93$ eV for IM1 sample is very similar to those obtained for low temperature GaAs (0.88–0.92 eV) although LT1–LT5 samples were produced with a different method. The same similarity is clearly visible in a comparison of the σ_k' parameter, which for IM1 and LT1–LT5 varies in a range of $1.525\times10^9-1.635\times10^9$ m^{-1}. Since for $\sigma_k\to\infty$ one should expect a finite σ_k' in order to obtain $\mathbf{\Delta k}$-independent matrix element $\mathcal{M}$, the value of 1.6×10^9 m^{-1} may be presumably regarded as an estimate of σ_k' parameter in the limit of infinite disorder.

B. Model of independent electron-hole pairs

The electron-hole correlation in strongly doped materials may be neglected due to the screening of the Coulomb interaction. However, as shown in Fig. 1, the spectra of implanted samples need a more thorough approach which would include excitonic effects. The presented below excitonic model describes a bound electron-hole pair which is scattered coherently by the random potential.

1. Model of disorder

In the effective mass approximation the disorder is represented by the random field $V(\mathbf{r})$, which we choose to be Gaussian, i.e., characterized by its mean value $\langle V(\mathbf{r})\rangle_V$ (which we can put equal to zero by shifting the energy scale) and the autocorrelation function

$$W(|\mathbf{r}-\mathbf{r}'|)=\langle V(\mathbf{r})V(\mathbf{r}')\rangle_V, \tag{9}$$

where $\langle\cdots\rangle_V$ denotes the average with respect to the configurations of disorder, which should be distinguished from the thermal average $\langle\cdots\rangle=\mathrm{Tr}\{e^{-\beta\hat{H}}\cdots\}$. The assumption of a Gaussian disorder becomes exact in the limit of high concentration of weakly scattering centers. It also has to be stressed, that for such model of random field, the cumulant averages[33] of the order higher than two disappear. These features make our model applicable to the systems with high concentration of weakly scattering defects, while the well known approach based on Dyson's equation[34] becomes exact in the limit of very small impurity density.

The autocorrelation functions in our considerations is purely phenomenological—Gaussian noise, given by

$$W(\mathbf{r})=V_{\mathrm{r.m.s.}}^2\exp\left(-\frac{r^2}{L^2}\right), \tag{10}$$

characterized by energy $V_{\mathrm{r.m.s.}}$ and length scale L. In the following we will employ the Fourier transform of $W(\mathbf{r})$ defined by $\tilde{W}(\mathbf{q})$.

2. One particle spectral density

Let us consider a one band system described by the Hamiltonian

$$\hat{H}=\hat{T}+\hat{V}=\sum_{\mathbf{k}}\epsilon(\mathbf{k})a_{\mathbf{k}}^\dagger a_{\mathbf{k}}+\sum_{\mathbf{k},\mathbf{k}'}V_{\mathbf{kk}'}a_{\mathbf{k}}^\dagger a_{\mathbf{k}'}, \tag{11}$$

where $a_{\mathbf{k}}^\dagger$ and $a_{\mathbf{k}}$ are, respectively, creation and destruction operators in the basis of Bloch waves, and $V_{\mathbf{kk}'}$ are the matrix elements of the random potential taken between the Bloch plane waves.

The spectral density function for a noninteracting system is given by

$$A(\mathbf{k},\omega)=\left\langle\sum_n|\tilde{\Psi}_n(\mathbf{k})|^2\delta(\omega-E_n)\right\rangle_V, \tag{12}$$

where $\tilde{\Psi}_n(\mathbf{k})$ are the Fourier transforms of the wave functions obtained for different realizations of disorder. This quantity, which is crucial for our method, can also be obtained from the one particle Green's function. If we define the retarded Green's function as

$$g_{\mathbf{kk}'}^R(t)=-i\theta(t)\langle\{a_{\mathbf{k}}^\dagger,a_{\mathbf{k}}\}\rangle, \tag{13}$$

and its disorder averaged counterpart as $G^R(\mathbf{k},t)=\langle g_{\mathbf{kk}}^R(t)\rangle_V$, we arrive at the well known expression for the spectral density

$$A(\mathbf{k},\omega)=-\frac{1}{\pi}\,\mathrm{Im}\,G^R(\mathbf{k},\omega), \tag{14}$$

where the Fourier transformed Green's function appears.

To calculate the disorder averaged correlation function we will use methods similar to those used in the stochastic differential equations theory. The solution of the equation fulfilled by g^R

$$\frac{\partial}{\partial t}g_{\mathbf{kk}'}^R(t)=-i\delta(t)\delta_{\mathbf{kk}'}-i\sum_{\mathbf{q}}H_{\mathbf{kq}}g_{\mathbf{qk}'}^R(t), \tag{15}$$

can be written as

$$g_{\mathbf{kk}}^R(t)=-i\theta(t)e^{-i\epsilon(\mathbf{k})t}\left[\mathcal{T}\exp\left(-i\int_0^t V(t')\right)\right]_{\mathbf{kk}}, \tag{16}$$

where $V(t)=e^{iTt}Ve^{-iTt}$, $\mathcal{T}$ is the chronological ordering operator and the fact that the matrix $\hat{T}$ is diagonal in the plane waves basis has been used to perform the matrix multiplication.

Now we average the above expression by performing the cumulant expansion to the second order with respect to $V(t)$ arriving at

$$G^R(\mathbf{k},t) = -i\theta(t)e^{-i\epsilon(\mathbf{k})t} \times \left[\exp\left(-\int_0^t dt_1 \int_0^{t_1} dt_2 \langle V(t_1)V(t_2)\rangle_V\right)\right]_{\mathbf{kk}}, \tag{17}$$

where $\langle V(\mathbf{r})\rangle_V = 0$ has been assumed.

After simple manipulations we obtain the following compact formula;

$$A(\mathbf{k},\omega) = \frac{1}{2\pi}\mathcal{L}_{\mathbf{k}}[\omega - \epsilon(\mathbf{k})], \tag{18}$$

where

$$\mathcal{L}_{\mathbf{k}}(\omega) = \int_{-\infty}^{+\infty} dt e^{i\omega t} e^{S(\mathbf{k},t)} \tag{19}$$

and

$$S(\mathbf{k},t) = \int_{-\infty}^{+\infty} d\omega \frac{e^{-i\omega t} + i\omega t - 1}{\omega^2} \mathcal{B}_{\mathbf{k}}(\omega). \tag{20}$$

The function $\mathcal{B}_{\mathbf{k}}(\omega)$ depends on the choice of the disorder autocorrelation function and is given by

$$\mathcal{B}_{\mathbf{k}}(\omega) = \frac{1}{(2\pi)^3}\int d^3q \tilde{W}(\mathbf{q}-\mathbf{k})\delta\{\omega - [\epsilon(\mathbf{q}) - \epsilon(\mathbf{k})]\}. \tag{21}$$

The form of the time-dependent *action* in Eq. (20) is well-known in the probability theory and the resulting spectral density function belongs to so-called infinitely divisible distributions,[35] so it is positively definite and normalized to unity [as long as the $\mathcal{B}_{\mathbf{k}}(\omega)$ function is positive and sufficiently regular, which is the case here].

Using the spectral densities we can calculate the disorder averaged DOS

$$N(E) = \int \frac{d^3\mathbf{k}}{(2\pi)^3} A(\mathbf{k},E). \tag{22}$$

Examples of densities of states calculated for the disorder autocorrelation function given by Eq. (10) are presented in Fig. 2. The mass of $0.5m_0$ has been used. The parabolic tail growing with disorder strength is clearly visible. It is worth noting, that after plotting the results from Fig. 2 in the logarithmic scale one can see the exponential tail spanning from three to five decades (depending on the numerical effort). It should be stressed that this is not the Urbach tail, but the exponential tail of the delocalized states.

3. Absorption coefficient-independent particle model

Now we consider a two-band model without interaction, described by the Hamiltonian

$$\hat{H} = \hat{T} + \hat{V}, \tag{23}$$

where

$$\hat{T} = \sum_{\mathbf{q}} \epsilon_c(\mathbf{q}) a^\dagger_{c\mathbf{q}} a_{c\mathbf{q}} + \sum_{\mathbf{q}} \epsilon_v(\mathbf{q}) a^\dagger_{v\mathbf{q}} a_{v\mathbf{q}}, \tag{24}$$

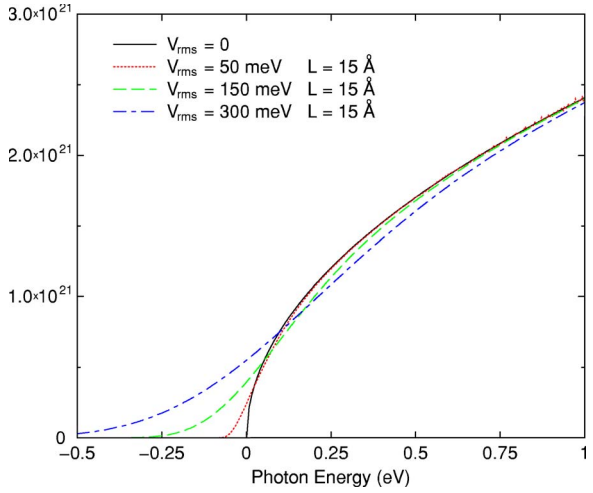

FIG. 2. (Color online) DOS for the Gaussian autocorrelation function with $L = 15$ Å and $V_{\text{r.m.s.}}$ ranging from 50 to 300 meV. Disorderless square-root DOS is plotted for reference.

$$\hat{V} = \sum_{\mathbf{q},\mathbf{q}'} (V^c_{\mathbf{qq}'} a^\dagger_{c\mathbf{q}} a_{c\mathbf{q}'} + V^v_{\mathbf{qq}'} a^\dagger_{v\mathbf{q}} a_{v\mathbf{q}'}). \tag{25}$$

Bands are spherical and parabolic

$$\epsilon_c(\mathbf{q}) = \frac{q^2}{2m_c} - \mu, \tag{26}$$

$$\epsilon_v(\mathbf{q}) = -\frac{q^2}{2m_v} - \mu - E_g. \tag{27}$$

Introducing the two-particle Green's function g and its disorder averaged counterpart $G = \langle g\rangle_V$ defined as

$$g^R_{\mathbf{kk}'\mathbf{k}'}(t) = -i\theta(t)\langle[a^\dagger_{v\mathbf{k}}(t)a_{c\mathbf{k}}(t), a^\dagger_{c\mathbf{k}'}a_{v\mathbf{k}'}(0)]\rangle, \tag{28}$$

we obtain the following expression for the absorption coefficient α as a function of photon frequency in atomic units:

$$\alpha(\omega) = -\frac{4\pi}{nc\omega\mathcal{V}} \text{Im} \sum_{\mathbf{kk}'} G^R_{\mathbf{kk}'\mathbf{k}'}(\omega) p^*_{cv}(\mathbf{k}) p_{cv}(\mathbf{k}'), \tag{29}$$

where n is the material refractive index, c is the speed of light in vacuum, $\mathcal{V}$, the volume of the system, $p_{cv}(\mathbf{k})$ is the interband dipole matrix element between the Bloch states of the wave vector $\mathbf{k}$ and $G^R_{\mathbf{kk}'\mathbf{k}'}(\omega)$ is equal to the Fourier transform of the time dependent, averaged Green's function.

To calculate this quantity we will use the analogous method as in the preceding section. Apart from the more complicated structure of the Hamiltonian the only difference is the appearance of the nontrivial boundary condition for the two-particle Green's function, so that the general solution of the equation of motion fulfilled by the correlation function can be written as

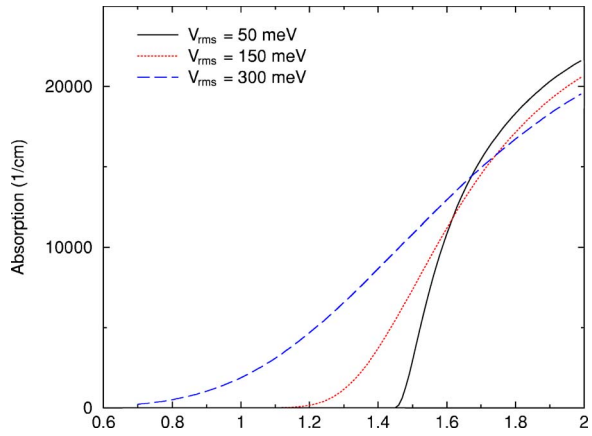

FIG. 3. (Color online) Absorption for the Gaussian autocorrelation function with $L=15$ Å and $V_{\mathrm{r.m.s.}}$ ranging from 50 to 300 meV.

$$g^R(t) = -i\theta(t)e^{-i\hat{T}t}\left[\mathcal{T}\exp\left(-i\int_0^t \hat{V}(t')dt'\right)\right]g^R(0), \tag{30}$$

where the matrix multiplication is implied, with all the quantities understood as matrices labeled by pairs of indices, i.e., $g^R_{\mathbf{kk}',\mathbf{qq}'}$.

In order to average with respect to disorder the above expression we assume the separation of the averages of the boundary condition and the time-dependent part. This ansatz yields after simple manipulations the following form of G^R:

$$G^R_{\mathbf{kkk}'\mathbf{k}'}(t) = -i\theta(t)\delta_{\mathbf{kk}'}e^{-i[\epsilon_c(\mathbf{k})-\epsilon_v(\mathbf{k})]t}e^{S_c(\mathbf{k},t)+S_v(\mathbf{k},-t)} \times[\langle\langle\hat{n}_{v\mathbf{k}}\rangle\rangle_V - \langle\langle\hat{n}_{c\mathbf{k}}\rangle\rangle_V], \tag{31}$$

where $\langle\langle\hat{n}_{\mathbf{k}}\rangle\rangle_V = \langle\langle a^\dagger_{\mathbf{k}}a_{\mathbf{k}}\rangle\rangle_V$, from which, using Eq. (29), we get the physically transparent formula for the absorption coefficient

$$\alpha(\omega) = \frac{16\pi^2P^2}{3nc\omega}\int\frac{d^3k}{(2\pi)^3}\int d\omega' A_c(\mathbf{k},\omega+\omega')A_v(\mathbf{k},\omega') \times[\langle\langle n_{v\mathbf{k}}\rangle\rangle_V - \langle n_{c\mathbf{k}}\rangle_V], \tag{32}$$

where the constant value of the interband matrix element $p_{cv}(\mathbf{k})=P$ has been used.

The last step in our derivation is the approximation for the disorder-averaged occupation factors $\langle\langle\hat{n}_{\mathbf{k}}\rangle\rangle_V$, for which we use the standard formula

$$\langle\langle n_k\rangle\rangle_V = \int d\omega A(\mathbf{k},\omega)n_{\mathrm{FD}}(\omega), \tag{33}$$

where $n_{\mathrm{FD}}(\omega)$ is the Fermi-Dirac occupation factor. Although it can be shown that our approach breaks the Kubo-Martin-Schwinger condition for the correlation functions, the above expression should be accurate enough when used in Eq. (32), where the occupation factors close to the energy shell are only needed.

The absorption spectra obtained by our method are shown in Fig. 3. Again the model Gaussian autocorrelation has been used with masses $m_v=0.5m_0$ and $m_c=0.067m_0$ which correspond to the valence and conduction band of GaAs. We note that the effect of closing the gap with increasing disorder, noticed above in Sec. IV A, is recovered by the model.

4. Excitonic effects

In order to describe the data for the implanted GaAs samples we adopt a model of excitons treated as composite particles scattered by the random potential. In the absence of free carriers they may be represented by exciton creation and annihilation operators

$$\mathbf{A}^\dagger_\lambda = \frac{1}{\mathcal{V}}\sum_{\mathbf{k}}\psi_{\lambda,\mathbf{k}}a^\dagger_{c\mathbf{k}}a_{v\mathbf{k}} \tag{34}$$

and

$$\mathbf{A}_\lambda = \frac{1}{\mathcal{V}}\sum_{\mathbf{k}}\psi^*_{\lambda,\mathbf{k}}a^\dagger_{v\mathbf{k}}a_{c\mathbf{k}}, \tag{35}$$

where the amplitude $\psi_{\lambda,\mathbf{k}}$ is equal to the Fourier transform of the excitonic hydrogenlike wave function corresponding to the state λ. Defining optical matrix element in this representation by

$$p_{cv}(\lambda) = \sum_{\mathbf{k}}\psi^*_{\lambda,\mathbf{k}}p_{cv}(\mathbf{k}), \tag{36}$$

we may rewrite the expression for the absorption coefficient in the form

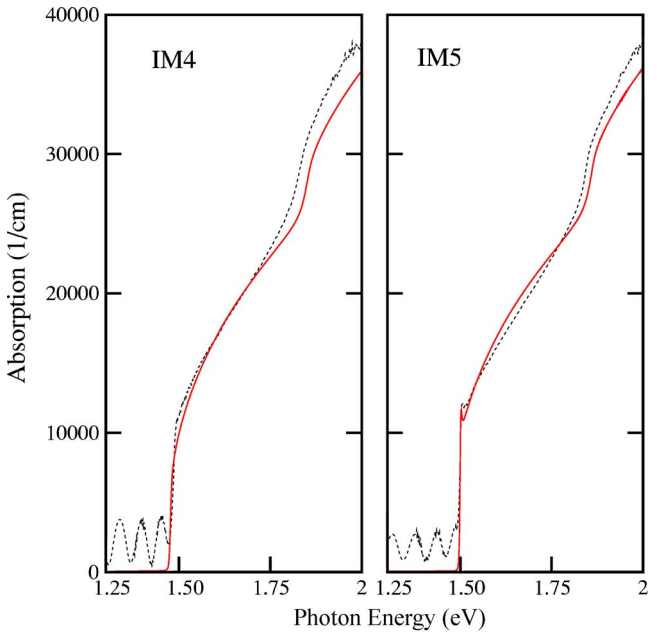

FIG. 4. (Color online) Theoretical (solid line) and experimental (dotted line) absorption curves for ion implanted GaAs samples IM4 and IM5. In both cases the correlation length $L=7$ Å is assumed while $V_{\mathrm{r.m.s.}}$ is equal to 130 meV for IM4 and 100 meV for IM5 sample.

$$\alpha(\omega) = -\frac{4\pi}{nc\omega\mathcal{V}} \operatorname{Im} \sum_{\lambda} G_{\lambda}^{R}(\omega)|p_{cv}(\lambda)|^2. \tag{37}$$

Here $G_{\lambda}^{R}(\omega)$ is equal to the Fourier transform of the time dependent exciton Green's function

$$G_{\lambda}^{R}(t) = -i\Theta(t)\langle\langle[\mathbf{A}_{\lambda}(t), \mathbf{A}_{\lambda}^{\dagger}(0)]\rangle\rangle_{V}, \tag{38}$$

which is approximately diagonal in the excitonic labels λ. Using analogous cumulant expansion procedure as in the derivation of the one particle Green's function in Eq. (31) we may approximately write

$$G_{\lambda}^{R}(t) = -i\theta(t)e^{-iE_{\lambda}t}e^{S_{\lambda}^{X}(t)}, \tag{39}$$

where E_{λ} denotes the energy of the exciton state λ while the complex phase $S_{\lambda}^{X}(t)$ results from the scattering of excitons by random potential. The final expression for the excitonic absorption is then obtained as

$$\alpha(\omega) = \frac{4\pi^2}{cn_r\omega}\sum_{\lambda} |p_{cv}(\lambda)|^2 \mathcal{A}_{\lambda}(\omega - E_{\lambda}) \tag{40}$$

in which $\mathcal{A}_{\lambda}(\omega) = \frac{1}{2\pi}\int_{-\infty}^{\infty} e^{S_{\lambda}^{X}(t)+i\omega t}dt$ is the spectral density function for an exciton in the state λ. We have performed simplified calculations in which we replaced the phase functions $S_{\lambda}^{X}(0,t)$ for each excitonic state by the electron-hole pair phase at fixed value of $\mathbf{k}=\mathbf{k}_0$ corresponding to the inverse of the effective Bohr radius of the exciton $S_{\lambda}^{X}(t) \approx S_c(\mathbf{k}_0, t) + S_v(\mathbf{k}_0, -t)$. We have also included in our calculations excitonic transitions from the spin-orbit valence subband. However, in order to describe the experimental data we had to add an additional broadening parameter which is due to the possibility of nonradiative decay via intersubband transitions.

The results of our theoretical calculations are compared to the experimental data obtained for the ion implanted GaAs samples IM4 and IM5 in Fig. 4. Reasonable overall matching between the experimental data and the model is apparent. In particular taking into account the electron-hole interaction allows to describe the features of absorption edge, which were not recovered by the RkR model (Fig. 1).

V. CONCLUSIONS

Our optical studies of disordered GaAs epilayers show that the ramplike fundamental absorption edge seems to be typical for nonstoichiometric materials, especially for samples grown with LT-MBE technique. In these systems the nonstoichiometry results from the well-known antisite As_{Ga} defect formation. In the case of GaAs implanted with As ions, we deal with excessive arsenic as well. For both types of GaAs we obtained reasonable matching of the RkR model with experimental data. However, the implanted samples spectra reveal the remnants of excitonic features which suggest a much lower level of disorder. In this case RkR phenomenological description of the fundamental absorption edge was successfully supported by the microscopic considerations employing the cumulant expansion method which should be valid in the presence of many weakly scattering centers.

The similar ramplike absorption edge was observed for $Ga_{1-x}Mn_xAs$ layers obtained by the LT-MBE method as well. Except arsenic antisites, which are unavoidable defects for low-temperature growth regime, there is the additional source of disorder in these compounds: magnetic Mn ions. However, comparing the results of our analysis using RkR model to the data obtained by Szczytko *et al.* for $Ga_{1-x}Mn_xAs$ we may conclude that the main source of disorder and peculiar behavior of the fundamental absorption edge in this semimagnetic material is related to inherent defects created during LT growth, while the contribution of the Mn ions is less important.

ACKNOWLEDGMENTS

This work was partially supported by The Ministry of Scientific Research and Information Technology (Poland).

*Electronic address: Konrad.Dziatkowski@fuw.edu.pl

[1] C. Timm, J. Phys.: Condens. Matter **15**, R1865 (2003).
[2] J. L. Xu, M. van Schilfgaarde, and G. D. Samolyuk, Phys. Rev. Lett. **94**, 097201 (2005).
[3] L. Bergqvist, P. A. Korzhavyi, B. Sanyal, S. Mirbt, I. A. Abrikosov, L. Nordström, E. A. Smirnova, P. Mohn, P. Svedlindh, and O. Eriksson, Phys. Rev. B **67**, 205201 (2003).
[4] C. Timm, F. Schäfer, and F. von Oppen, Phys. Rev. Lett. **89**, 137201 (2002).
[5] L. Craco, M. S. Laad, and E. Müller-Hartmann, Phys. Rev. B **68**, 233310 (2003).
[6] H. Ohno, A. Shen, F. Matsukura, A. Oiwa, A. Endo, S. Katsumoto, and Y. Iye, Appl. Phys. Lett. **69**, 363 (1996).
[7] R. Shioda, K. Ando, T. Hayashi, and M. Tanaka, Phys. Rev. B **58**, 1100 (1998).
[8] A. Wołoś, M. Kamińska, M. Palczewska, A. Twardowski, X. Liu, T. Wojtowicz, and J. K. Furdyna, J. Appl. Phys. **96**, 530 (2004).
[9] G. D. Cody, J. Non-Cryst. Solids **141**, 3 (1992).
[10] G. Lasher and F. Stern, Phys. Rev. **133**, A553 (1964).
[11] F. Stern, Phys. Rev. B **3**, 2636 (1971).
[12] H. C. Casey, Jr. and F. Stern, J. Appl. Phys. **47**, 631 (1976).
[13] S. K. O'Leary, S. Żukotyński, and J. M. Perz, Phys. Rev. B **51**, 4143 (1995); **52**, 7795 (1995).
[14] I. D. Desnica-Frankovic, Philos. Mag. B **82**, 1671 (2002).
[15] S. K. O'Leary, Appl. Phys. Lett. **72**, 1332 (1998).
[16] Th. Flohr and R. Helbig, J. Non-Cryst. Solids **88**, 94 (1986).
[17] J. Szczytko, W. Bardyszewski, and A. Twardowski, Phys. Rev. B **64**, 075306 (2001).
[18] S. U. Dankowski, D. Streb, M. Ruff, P. Kiesel, M. Kneissl, B. Knüpfer, G. H. Döhler, U. D. Keil, C. B. Sørenson, and A. K. Verma, Appl. Phys. Lett. **68**, 37 (1996).
[19] F. W. Smith, A. R. Calawa, C. L. Chen, M. J. Mantra, and L. J. Mahoney, IEEE Electron Device Lett. **9**, 77 (1988).
[20] A. Claverie, F. Namavar, and Z. Liliental-Weber, Appl. Phys.

Lett. **62**, 1271 (1993).
[21] G.-R. Lin and C.-L. Pan, Jpn. J. Appl. Phys., Part 1 **40**, 6226 (2001), and references therein.
[22] P. K. Chakraborty, L. J. Singh, and K. P. Ghatak, J. Appl. Phys. **95**, 5311 (2004).
[23] S. Marcinkevicius, C. Jagadish, H. H. Tan, M. Kaminska, K. Korona, R. Adomavicius, and A. Krotkus, Appl. Phys. Lett. **76**, 1306 (2000).
[24] At room temperature the spectra of LT1–LT5 samples are shifted for about 80–90 meV into the lower photon energy region as compared with results obtained at 12 K. In a case of IM1–IM5 samples the spectra are shifted for about 40–80 meV.
[25] The curvature and noises visible above 1.9 eV are the results of insufficient sensitivity of the apparatus for such large absorbance.
[26] M. Kaminska, M. Skowronski, and W. Kuszko, Phys. Rev. Lett. **55**, 2204 (1985).
[27] P. Omling, E. R. Weber, and L. Samuelson, Phys. Rev. B **33**, 5880 (1986).
[28] Landolt-Börnstein, *Numerical Data and Functional Relationships in Science and Technology* (Springer-Verlag, Berlin, 1982), Vol. III/7a.
[29] For another model considering the wave-vector dependence of the optical matrix element see Ref. 22.
[30] In other words, the function $\sigma_k'(\sigma_k)$ saturates for $\sigma_k \to \infty$.
[31] Here we take $\Delta_{SO}=0.34$ eV according to Ref. 28.
[32] T. Tomaru, T. Uchiyama, C. T. Taylor, S. Miyoki, M. Ohashi, K. Kuroda, T. Suzuki, A. Yamamoto, and T. Shintomi (unpublished).
[33] R. Kubo, J. Phys. Soc. Jpn. **17**, 1100 (1962).
[34] W. Kohn and J. M. Luttinger, Phys. Rev. **108**, 590 (1957).
[35] W. Feller, *An Introduction to Probability Theory and Its Applications*, 3rd ed. (Wiley, New York, 1967), Vol. II.